Multi-walled Carbon Nanotubes/Silicone Conductive Foams and Their Piezoresistive Behaviors

Chen Guo [1]; Yasuo Kondo [2]; Chika Takai [1]; Masayoshi Fuji [1*]

[1] Advanced Ceramics Research Center, Nagoya Institute of Technology, Tajimi, Japan

[2] R&D Division, Kitagawa Industries Co., Ltd., Kasugai, Japan

* E-mail: fuji@nitech.ac.jp Tel: +81-572-24-8110 Fax: +81-572-24-8109

Abstract

Multi-walled carbon nanotubes/silicone conductive nanocomposites are of great significance because of their unique electrical and mechanical properties and are expected to open up a new field of applications as smart functional materials. Especially their noticeable piezoresistive behaviors can be utilized to produce flexible tactile sensors with large sizes but low costs. To enhance the sensitivity of the piezoresistive property, a foaming procedure was introduced to the conductive polymeric composites. A series of novel multi-walled carbon nanotubes/silicone conductive foamed nanocomposites were fabricated with different types of foaming agents to obtain a diverse porous structure. The porous structures of the foams, the distribution and orientation state of the multi-walled carbon nanotubes in the silicone matrix were both observed using a laser microscope and SEM with or without a compressive load. The influences of the porous structure and porosity on the foam were studied. It was found that a different porosity and different voids structure affected the density, elastic modulus, resistivity as well as piezoresistive property significantly. A piezoresistive model for the conductive fillers reinforced elastomeric composites was developed, the calculated results of resistive variations were used to compare to the measured values. Although the overall trends of the resistance changes matched, notable separations were found between the theoretical values and the measured values, which are thought to be caused by the viscoelasticity of the silicone matrix.

Keyword: multi-walled carbon nanotube; piezoresistive property; porous structure; foaming efficiency; electrically conductive foam

1. Introduction

Carbon nanotube (CNT) is a type of cylindrical-like carbon nanomaterial with many unusual properties such as extraordinary thermal conductivity, mechanical and electrical properties which are valuable in many structural and functional applications [1-5]. Especially the multi-walled carbon nanotube (MWCNT) has a relatively low cost and many special behaviors [6-8]. Carbon nanotube has metallic conductivity or semiconducting behavior along its tubular axis. In theory, an armchair type carbon nanotube can carry an electric current density about 1000 times greater than that of copper [9]. Thus CNTs are famous for being investigated as conductivity enhancing fillers in polymeric composites. J. O. Aguilar et al. studied the influence of CNT clustering on the electrical properties of polymer composite films by comparing the composites with CNTs uniformly dispersed and with those agglomerated in clusters at micro-scale. They found that films with micrometer-size agglomerations have a slightly lower percolation threshold and a higher conductivity than those with uniformly dispersed CNTs, which can be explained that the increased density of CNT-to-CNT junctions favor the formation of the conductive networks [10].

The demand for diverse types of sensors with smart property and low cost is growing rapidly as the recent development of novel technologies especially artificial intelligence (AI), virtual reality (VR), bionics and biotechnology. Many previous works have been conducted for the implementation of nanocomposites in advanced sensor applications [11-17]. M. L. Yola et al. developed a novel imprinted electrochemical biosensor based on Fe@AuNPs and f-MWCNs for direct determination of cefexime (CEF) in human plasma, which showed high sensitivity and selectivity towards CEF and offers the advantages of simplicity and efficiency in target detection from biological samples [11]; their groups also reported the synthesis and application of NiO-multiwall carbon nanotube nanocomposite (NiO/MWCNTs) and 1-butyl-3-methylimidazolium tetrafluoroborate ([Bmim]BF4) in the carbon paste matrix as high sensitive sensors for voltammetric determination of vitamin C in the presence of vitamin B9 in food and drug samples [12]; a robust micro-vibration sensor for biomimetic fingertips was designed by J. A. Fishel et al., which can readily detect the high frequency vibrations by recording the fluid conducted vibration signals when such a fingertip slides across a ridged surface [13].

MWCNT/polymer conductive nanocomposites have many unique electrical and mechanical properties, such as piezoresistivity, EMI shielding effect and highly flexibility, which are appropriate for applications as smart functional materials. MWCNT/polymer conductive nanocomposites offer obvious piezoresistive behaviors and can be easily produced to large sizes with very low costs and be utilized to many special fields due to their highly flexibility. The strain-dependent electrical resistance characteristics of MWCNT/polyethylene oxide (PEO) were investigated in the research of Park, M. et al. Unique and repeatable relationships in resistance versus strain were obtained, the overall pattern of which was found consists of linear and nonlinear regions. This type of material was expected to be used as tunable strain sensors such as sensors embedded into systems [18]. Al-Saleh et al. analyzed the EMI shielding mechanisms of MWCNT/polypropylene composite plates experimentally and theoretically, found that the absorption is the major shielding mechanism and the reflection is the secondary shielding mechanism. A negative influence on the overall EMI shielding effectiveness brought by multiple-reflection was shown by the theoretical analysis. They believed that a multi-surface shield such as conductive polymer composites might drastically enhance the overall EMI shielding effectiveness if multiple-reflection can be minimized [19]. The piezoresistive properties of MWCNT/polymer solid composites have been reported by many previous works. As an important method to enhance the sensitivity of the piezoresistive property, foaming process has been widely used to the conductive nanocomposites in industry. However, there is almost no report about the piezoresistive properties of foamed MWCNT/polymer composites from other research groups. In this study, a series of novel MWCNT/silicone conductive foamed nanocomposites were fabricated. The diverse porous structures, the distribution and orientation states of the MWCNTs in the silicone matrix were observed by a laser microscope and SEM with or without a compressive load. The influences of the porous structure and porosity on the foam density, elastic modulus, resistivity as well as piezoresistive property were studied. A piezoresistive model for the foamed conductive fillers reinforced elastomeric composites was developed, the calculated results of the resistive variations were used to compare to the measured values.

2. Theoretical Model for Piezoresistance of the Conductive Foam

Various theoretical electrically conductive models and piezoresistive models have been developed in many previous works [20-22]. In M. Taya' work, an analytical modeling was developed to study the piezoressitive behavior of a

conductive short fiber reinforced elastomer composite, the reorientation distributions of the conductive short fibers due to stretching straining were computed by using a fiber reorientation model. It was found that the threshold fiber volume fraction increases as the applied strain increases [23]. An analytical model of effective electrical conductivity of carbon nanotube composites was developed by Fei Deng et al., which takes account of not only the CNT concentration and percolation, but also CNT conductivity anisotropy, aspect ratio and nonstraightness [24].

In the works of Xiang-wu Zhang [25,26], the total resistance in conductive composites is considered to be a function of both the resistance through each conducting particle and the polymer matrix. The resistivity of the matrix is assumed to be constant everywhere, the resistance of the conductive paths perpendicular to the current flow was neglected. Then the number of the conductive particles between electrodes, the number of the conducting paths and the average distance between the adjacent particles become the main factors, the resistance for the conductive composites can be described as

$$R = \frac{M}{N}\left[\frac{8\pi hs}{3A\gamma e^2}\exp(\gamma s)\right] \quad (1)$$

where

$$\gamma = \frac{4\pi}{h}\sqrt{2m\varphi}$$

here s is the average minimum distance between two adjacent conductive particles, A is the effective cross-sectional area of one electrically conducting path, h is Plank' constant, e and m are the electron charge and electron mass, φ is the tunneling potential barrier height, N is the number of conducting paths in the composite and M is the number of conductive particles forming one conducting path. If the initial average minimum distance between two adjacent conductive particles and the initial resistance is assumed as s_0 and R_0, respectively, the relative resistance of the conductive composites when a stress is applied can be described as

$$\frac{R}{R_0} = \frac{s}{s_0}\exp[\gamma(s - s_0)] \quad (2)$$

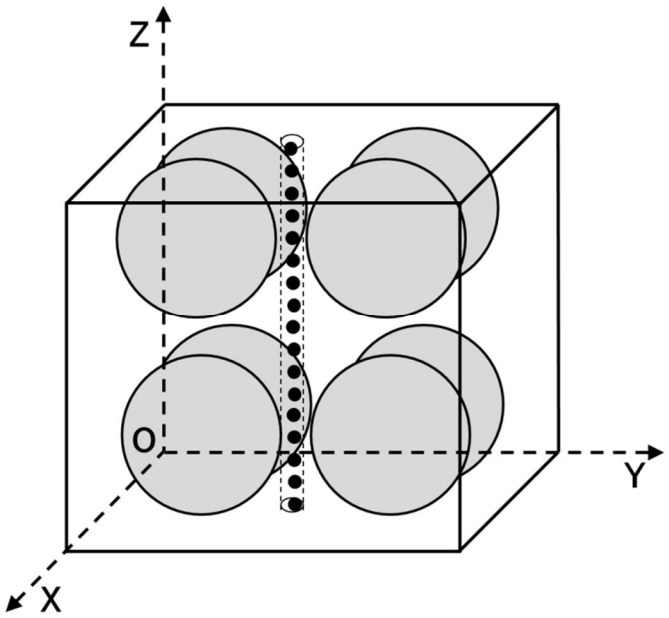

Fig.1 An image of an electrically conductive path in a cubic space of the conductive foamed composite

Considering the situation of the conductive foam, the compression could become much more complex because of the influence of the porous structure on the elastic modulus. A cubic space in the conductive foam with a length of L was illustrated in the Fig.1. Both voids and conductive particles were assumed as spherical shapes and to be distributed in the polymer matrix with absolutely homogeneities. The voltage was loaded from the electrodes parallel with the XOY plane, thus the current went through the ZO direction. The current was thought homogeneously distributed in the space where was not blocked by the voids through the ZO direction. One of the conducting paths was shown in the Fig.1, which was thought to keep being perpendicular to the XOY plane. If a uniaxial pressure is loaded on the conductive foam through the ZO direction, the cubic space will be compressed, the average distance between the conductive particles would be shortened and the resistance of the conductive foam through the ZO direction would be reduced. However, the influence of the voids on the compressing procedure is extremely complex, making it difficult to calculate the piezoresistive property of the conductive foam.

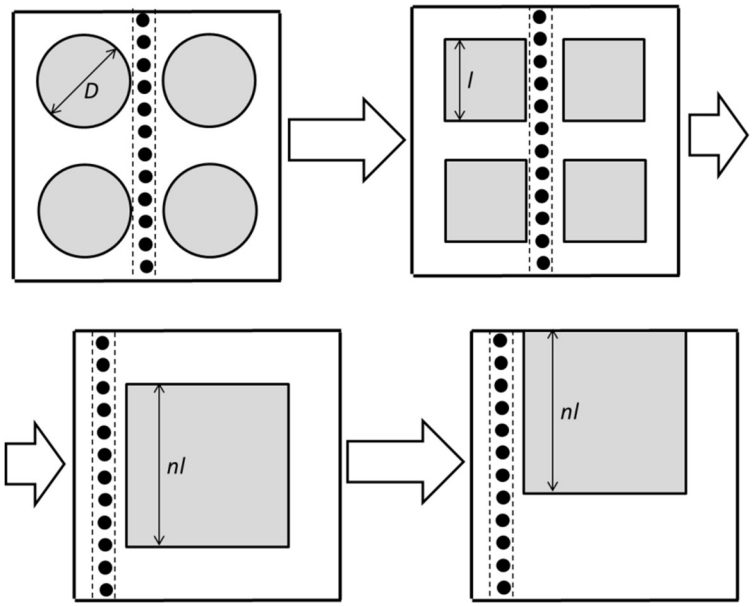

Fig.2 The flow chart of simplification of the piezoresistance analysis of a cubic space in the conductive foamed composite

In order to simplify the calculation procedures, several assumptions were made for the voids. (1) The spherical voids with an average diameter D were treated as cubic voids with an average length of l and maintain a constant average volume. As shown in the Fig.2, the XOZ (or YOZ) plane from the Fig.1 was illustrated. One electrically conductive path through the ZO direction was shown in the Fig.2. Thus it can be known that

$$\frac{\pi}{6}D^3 = l^3$$

$$l = \left(\frac{\pi}{6}\right)^{1/3} D$$

(2) The effect of the pressure of confined gas in the voids and the atmospheric pressure on the compressing procedure was neglected.

(3) The number of the conductive particles within one conductive path in the cubic space was expressed as *n*. These cubic-like voids in this cubic space were assumed to be combined together as a big cubic-like void, which has a length of *nl*. This big void can be moved freely within the cubic space without affecting the calculation of the piezoresistive property due to the cubic shape. Then it was assumed to be moved to the top of the cubic space, dividing the space into a "hollow" part upper and a "solid" part inferior. The length of the big cubic-like void is

$$nl = \sqrt[3]{\frac{(1-\rho_r)L^3}{l^3}} \cdot l = (1-\rho_r)^{\frac{1}{3}} \cdot L = kL$$

Thus the ratio of the length of the big cubic void versus the length of the entire cubic space can be calculated as

$$k = \frac{nl}{L} = (1-\rho_r)^{1/3} \quad (3)$$

Here ρ_r is the relative density of the conductive foam (the density of the conductive foam divided by the density of the solid conductive composites with the same volume fraction of conductive particles). *l* is the length of a single void before combination and L is the length of the big void after combination, respectively.

When an external force was loaded on the cubic space though the ZO direction, the compressive strain of the upper "hollow" part ε_h and the compressive strain of the inferior "solid" part ε_s were different because of the different force loaded areas. Considering this difference and neglecting the compression of the conductive particles, the particle separation *s* in the conductive foam can be calculated as

$$s = s_0[1-\varepsilon_h-\varepsilon_s] = s_0\left[1-\left(1-k+\frac{k}{1-k^2}\right)\frac{\sigma}{E}\right] \quad (4)$$

where σ is the applied uniaxial stress, *E* is the elastic modulus of the solid conductive composites with the same volume fraction of conductive particles. The inter-particle separation can be calculated as

$$s_0 = d\left[\left(\frac{\pi}{6}\right)^{1/3}\left(\frac{f}{\rho_r}\right)^{-1/3}-1\right] \quad (5)$$

where *d* is the average particle diameter, *f* is the volume fraction of the conductive particle in the conductive foam, f/ρ_r is thought as the "real" volume fraction in the polymer matrix. Then substitute the equations (4) and (5) into the equation (2), the relative resistance of the conductive foam when a stress is applied can be calculated as

$$\frac{R}{R_0} = \left[1-\left(1-k+\frac{k}{1-k^2}\right)\frac{\sigma}{E}\right]\exp\left[-\frac{\sigma\gamma s_0}{E}\left(1-k+\frac{k}{1-k^2}\right)\right] \quad (6)$$

The piezoresistive property can be simply estimated with the equations (6). This piezoresistive model can be used to predict the effect of the porosity of the conductive foam on its piezoresistance effectively. However there are some drawbacks in this model which would reduce the accuracy of the prediction: (1) The pores in the conductive foam were considered as cubic shapes, which have a different compression mode with the spherical one. Furthermore, the average pore diameter was neglected due to the combination of the pores; (2) The competition between the pressures of the gas confined in the pores and the atmospheric pressure was neglected, which in fact brings some effect on the compressing procedures; (3) The electrically conductive particles were assumed to be spherical shapes. In fact, many fiber-like or sheet-like conductive particles were found to have lower percolation thresholds and much more effective for conductivity enhancing compared to the spherical particles. In our previous work [27], piezoresistive models for fiber-like conductive fillers/polymeric solid composites and for fiber-like fillers/polymeric foam were both developed. Those models were

designed to reflect the effects of both the displacement and orientation of the fiber-like fillers precisely, although lead to some extremely complex calculation and thereby reduce the practicability. In this study, the equation (6) accompanied with (3) and (5) was used to calculate the piezoresistive variations of the MWCNT/silicone conductive foams and the results were used to compared to the measured values in the later chapter.

3. Experimental Section

3.1 Materials

A type of multi-walled carbon nanotube (VGCF-H, Showa Denko) with an average fiber length of 10~20μm and an average fiber diameter of 150nm was used as the conductive filler. The polymer matrix was synthesized by 2-component silicone elastomer, including the main component (KE-1308, Shin-Etsu Chemical Co., Ltd.) and the curing agent (CAT-1300L-4, Shin-Etsu Chemical Co., Ltd.). 3 types of foaming agents were used, including an OBSH type with a main component of 4,4'-Oxybis (benzenesulfonylhydrazide) (CELMIC S, SANKYO KASEI CO., LTD.), an ADCA type with a main component of Azodicarbonamide (M-35, Otsuka Chemical Co., Ltd.) and a inorganic carbonate type with a main component of Sodium Hydrogen Carbonate (P-5, Otsuka Chemical Co., Ltd.).

3.2 Sample Preparation

Firstly, all the components of the silicone elastomer were added to a PTFE container according to an expected ratio (the curing agent was added at an amount of 6% of the main component by mass). Then the foaming agent and the MWCNT were also added. The mixture was finely stirred using a planetary centrifugal vacuum mixer at a speed of 1000rpm at a pressure of 0.6kPa for 10min and then poured into a mold immediately, the composite membrane before foaming was obtained after curing at 110˚C for 5min. Finally, the conductive MWCNT/silicone foam was obtained by free foaming for 10min at 170˚C in vacuum. The thicknesses of these foams were controlled approximately to 4mm. Foam structures with closed voids were obtained, the shapes of the voids vary with the types of the foaming agents. The volume fractions of MWCNT and foaming agent (before foaming) were listed in Table 1. Each type of foaming agent was added to the silicone matrix with two different volume fractions to investigate the effect of the porosity on the piezoresistive properties.

Table1 Volume fractions of the MWCNT and foaming agents in the MWCNT/silicone conductive foams

Component \ Series Number		O1	A1	S1	O2	A2	S2
MWCNT		4.16%	4.19%	4.13%	4.21%	4.25%	4.16%
Foaming Agents	OBSH	5.95%	-	-	9.05%	-	-
	ADCA	-	5.33%	-	-	8.16%	-
	$NaHCO_3$	-	-	6.69%	-	-	10.11%

3.3 Characterization

The volume resistivity was measured by an ADVANTEST R6243 DC voltage current source/monitor with a 4-wired method; the laser microscope observation was conducted by an OLYMPUS LEXT OLS4000 3D measuring laser microscope; the SEM observation was applied at an accelerating voltage of 15kV by a JEOL JSM-7600F field emission scanning electron microscope (The cross sections of the samples for these observations were obtained by breaking them

after freezing in liquid nitrogen. Each sample was loaded with a uniaxial pressure through the thickness direction by a pair of metallic plates set into the sample holder, the compressing strain was controlled to 0 and 75%). The elastic modulus was measured by a SHIMADZU AGS-G Series Universal/Tensile Tester, with a compressing speed of 3mm/min.

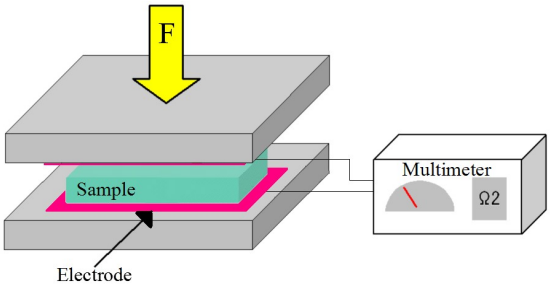

Fig.3 Piezoresistivity measurements through the vertical direction

The piezoresistive properties were measured though the direction parallel to the external pressure. Each sample was cut to a square-shape sheet of 30mm×30mm. The measurement was shown in the Fig.3. Every sample was sandwiched between a pair of 75mm×75mm square-shape copper electrodes. A linear-increasing uniaxial pressure was loaded by a compressing plate, which was controlled by the SHIMADZU AGS-G Series Universal/Tensile Tester. Silver paint was smeared to the sample surfaces to ensure a well surface contact with the electrodes. The electrodes were connected to a 2000 Series Digit Multimeter to measure the resistance with a 2-wire mode. For every sample, the resistance was measured under difference stress from 0 to 112kPa and listed as the form of common logarithms.

4. Results and Discussion

4.1 Density and Resistivity (4-wired method) Measurements

Table2 Density and resistivity of MWCNT/silicone conductive foams

Series Number	O1	A1	S1	O2	A2	S2
Density ($g \cdot cm^{-3}$)	0.55	0.93	0.89	0.41	0.84	0.88
Resistivity ($\Omega \cdot m$)	5267.8	5.79	6.59	21922.8	9.62	13.74

The density and resistivity of MWCNT/silicone conductive foams were listed in the Table2. It can be found that the O1 and O2 samples have the lowest densities and the highest resistivity, which means that the OBSH foaming agent has the highest foaming efficiency. With increasing of the foaming agents, the density decreases and the resistivity increases obviously for all samples. It is believed that a lower density, namely, a highly porous structure leads to a higher resistivity. It is also found that the OBSH foaming agent effectively increased the percolation threshold of the MWCNT/silicone composites, making the resistivity increase significantly. For the A1 and A2 samples, with increasing of the foaming agent, the density decreases but the resistivity keeps at a same level. For the S1 and S2 samples, an obvious change can be observed from neither the density nor the resistivity with increasing of the foaming agent. Only relatively low foaming efficiencies and weak conductivity-reducing effects could be brought by the ADCA and $NaHCO_3$ foaming agents.

4.2 Laser Microscope Observation

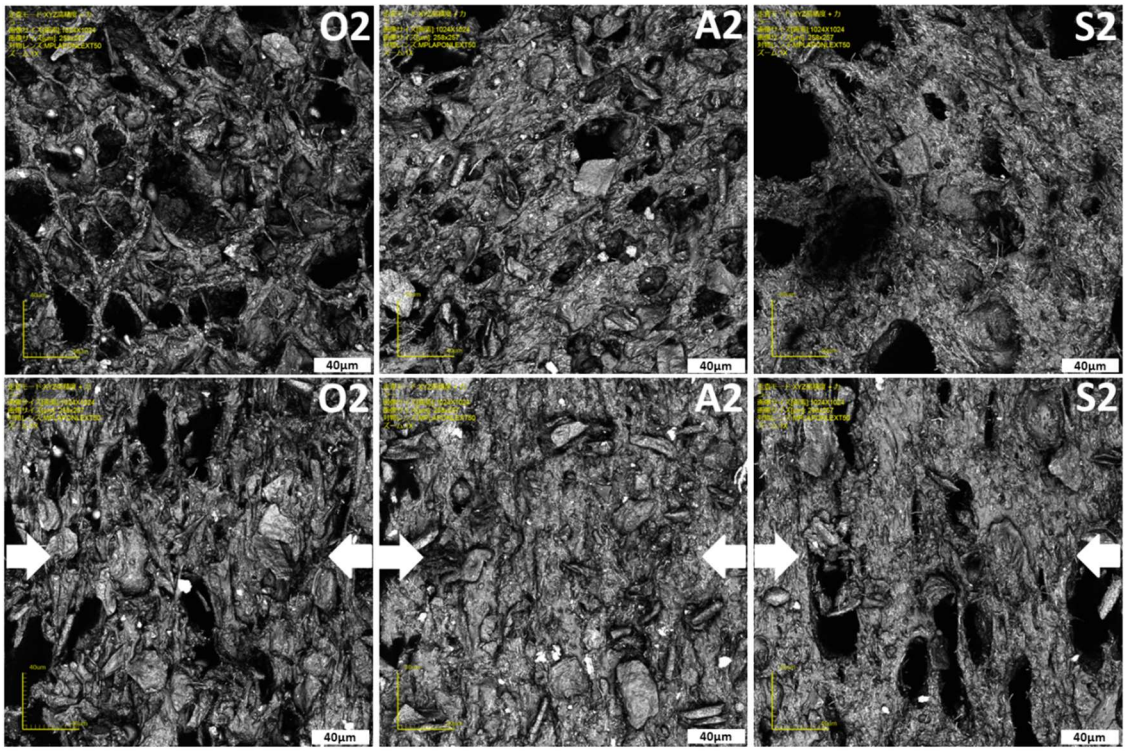

Fig.4 Laser microscope images of the porous structures in MWCNT/silicone conductive foams with and without a uniaxial load

The cross-sectional area of the conductive foam samples of O2, A2 and S2 series were observed by the laser microscope. The porous structures with many closed-cell pores can be clearly observed from all samples. The images of the MWCNT/silicone conductive foams without a compressing strain were shown in the upper parts of the Fig.4. Small voids can be found from the O2 and A2 samples, which were found to be crowded in the former one and loose in the latter one, meanwhile large voids with a small amount were found in the S2 samples. The reason of the diverse porous structures was considered as follows: (1) the OBSH foaming agent has a relatively lower molecular polarity and has been surface treated previously to gain a well affinity with the non-polar silicone matrix. After a high shearing mixing procedure, the clusters of the OBSH particles maintained relatively small sizes until absolutely curing. Furthermore, the OBSH is a type of compound with rather low decomposing temperature accompanied with a high decomposing speed and a relatively low gas releasing amount. Thus during the free foaming procedure, a dense and fine porous structure could be obtained with a short heating time; (2) the $NaHCO_3$ foaming agent has a relatively higher molecular polarity, which leads to a poor affinity with the silicone matrix. The clusters of the foaming agents would begin to agglomerate bigger and bigger after the high shearing mixing procedure. These big clusters would release a large amount of gas and create big pores in the S2 sample; (3) although the ADCA foaming agent has a large gas releasing amount as twice as the OBSH and the $NaHCO_3$ foaming agent, the amino groups contained in its molecules are easy to react with the platinum

catalyst of the 2-component silicone matrix, which would obstruct the curing of the silicone matrix and disturb the foaming procedure, resulting in a lower porosity and a smaller average pore diameter.

The images of the MWCNT/silicone conductive foams under a compressing strain of 75% were shown at the bottoms of the Fig.4. For all samples, most of the voids were found crushed severely by the external pressures. Because the voids can be easily squashed, the elastic modulus was reduced greatly, making the compressive deformation much more obvious compared to the pure silicone matrix. At the same time, the variation range of the resistivity of the conductive composites was thought to be enlarged significantly due to the smaller elastic modulus.

4.3 SEM Observation

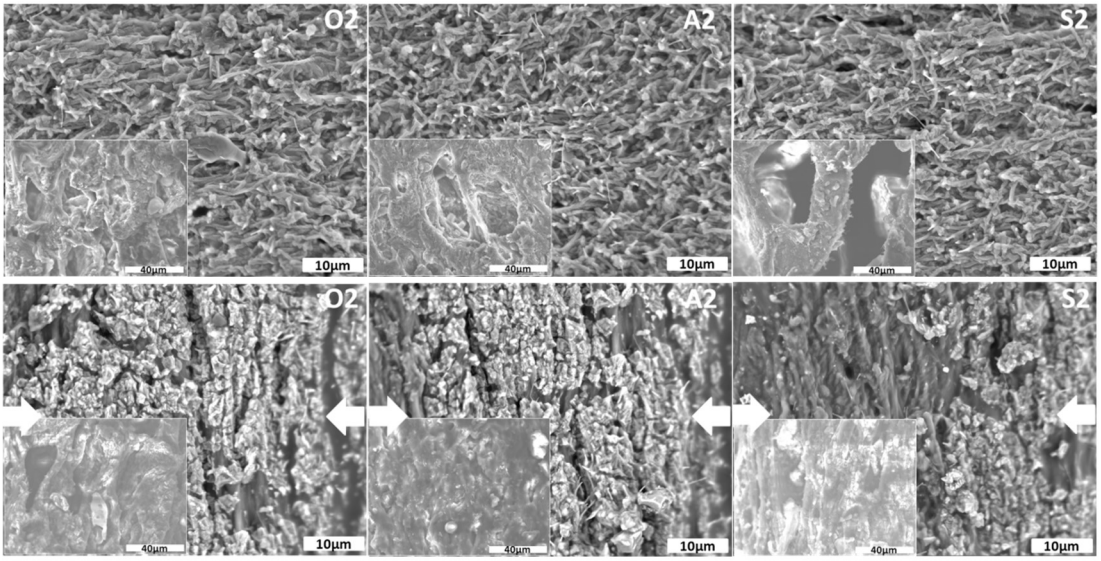

Fig.5 SEM images of the MWCNT/silicone conductive foams with and without a uniaxial load

The backscattered electron images of the MWCNT were taken at a high magnification while normal SEM images of the voids structures were taken with a low magnification. The images of the porous structures from all the foams were found similar with those obtained from the laser microscope observation, which convinced the observations of the laser microscope.

The images of the MWCNT/silicone conductive foams without a compressing strain were shown in the upper parts of the Fig.5. Large amounts of MWCNT particles were found being distributed homogeneously in the silicone matrix. The majority of which were covered tightly with silicone elastomer except for several half-naked particles distributed in the cross-section surface. These covered MWCNT particles contacted, overlapped each other and formed cluster-liked conductive networks. It is believed that the coated silicone layers hindered the direct contact between the MWCNT fibers, preventing the construction of the short circuit and making the resistivity of the conductive foams become much more changeable. It can be found that all the MWCNT fibers were distributed in the silicone matrix with random orientations before compression. The images of the MWCNT/silicone conductive foams under a compressing strain of 75% were shown in the inferior parts of the Fig.5, the majority of the MWCNT fibers were found being oriented to the direction perpendicular to the compressive strain, the contact and overlapping were dramatically enhanced by the external

pressures. This is considered to be the main enhancement factor of the piezoresistive phenomenon of the MWCNT/silicone conductive foams.

4.4 Compressive Elastic Modulus Measurement

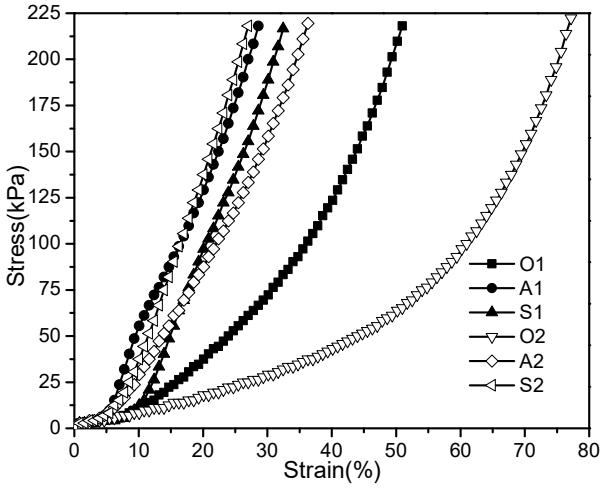

Fig.6 Compressive stress-strain curves of the MWCNT/silicone conductive foams

The compressive stress-strain curves were shown in the Fig.6. The slope of every point in a curve represents the elastic modulus of the conductive foam at that strain. In order to make the elastic results simple and quantitative, the average compressive elastic modulus during the whole strain range for one sample was calculated by the equation below. The results were listed in the Table3.

$$\bar{E} = \frac{2\int_0^{\varepsilon max}\sigma(\varepsilon)d\varepsilon}{(\Delta\varepsilon)^2} \quad (7)$$

Table3 Average compressive elastic modulus of the MWCNT/silicone conductive foams

Series Number	O1	A1	S1	O2	A2	S2
Elastic Modulus (kPa)	278.4	621.2	471	154.8	463.4	608.6

Evidently the O2 and O1 samples showed the lowest elastic modulus, which proved that the OBSH foaming agent has the best affinity with the silicone elastomer and the highest foaming efficiency. Relatively higher elastic modulus was found from the samples foamed with the ADCA and $NaHCO_3$ foaming agents, proving their lower foaming efficiencies. These results were found well matched with those from the density measurement. In addition, the stress-strain curves of the A series and S series samples were found to be almost linear. The reason was considered that the A or S series samples have a similar compressive procedure with solid conductive composites due to the low porosity, a procedure which obeys the Hook' law. Oppositely, highly porous structures found in the O series samples lead to a nonlinear,

complicated compressive mode. It was thought that the elastic modulus would decrease as the increase of all types of foaming agents. Unexpectedly, the elastic modulus of the conductive foam increased obviously as increasing of the $NaHCO_3$ foaming agent. The reason for which was considered that the $NaHCO_3$ foaming agent has a relatively low reaction rate, the unreacted foaming agent granules partially hindered the polymer chain movements of the silicone matrix and increased the elastic modulus.

4.5 Piezoresistance Measurement

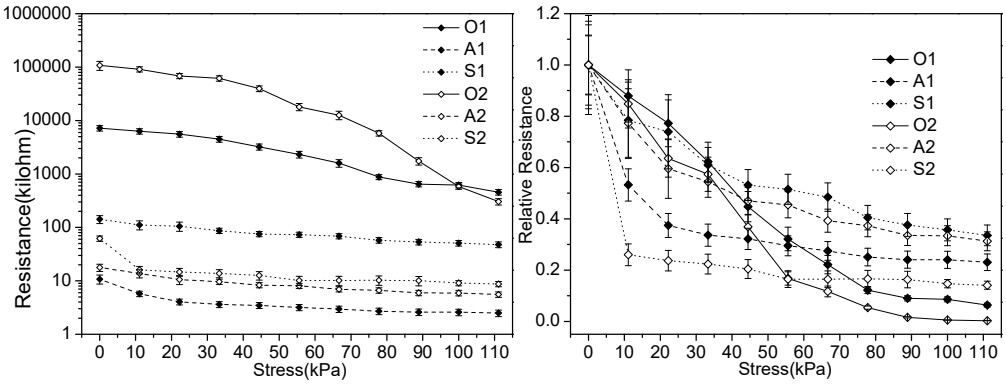

Fig.7 Piezoresistive properties of the MWCNT/silicone conductive foams

The piezoresistive properties of the MWCNT/silicone conductive foams with all types of foaming agents were shown in the Fig.7, the left-hand part of which illustrates the resistance-stress connections while the right-hand part of which shows the relative resistance-stress connections. Error bars have been included in the figure according to the measurement errors. The error range became narrower as the decrease of resistance due to the measurement property of the instrument. The resistance decrease can be found from all samples as the increase of the stress, almost all of the resistance-stress curves and relative resistance-stress curves were found to be nonlinear, which could be caused by their complex foam compression modes. Obvious deceases can only be found from the O1 and O2 samples especially from the latter one. This demonstrates that a lower elastic modulus brought by the foaming agent with a high foaming efficiency leads to a higher piezoresistive sensitivity, which can be enhanced simply by increasing the loading of the foaming agent. The relative resistances of the O1 and O2 samples dropped obviously when loaded with a uniaxial stress of about 110kPa. It is believed that the voids in the foams occupied much space of the silicone matrix, enlarged the distances between the MWCNT particles. Therefore the resistivity was increased significantly. The resistance changes of the O1 and O2 samples are precise and rapid enough to be utilized within a piezoresistive tactile sensor. Oppositely, only slight resistance decreases were obtained from A series and S series samples due to the relatively lower foaming efficiencies of the ACDA and the $NaHCO_3$ foaming agents. It is also noteworthy that the resistances maintained in higher ranges for samples O1 and O2 and in lower ranges for other samples. An obvious increase of the whole resistance range was brought to the silicone matrix by the OBSH foaming agent.

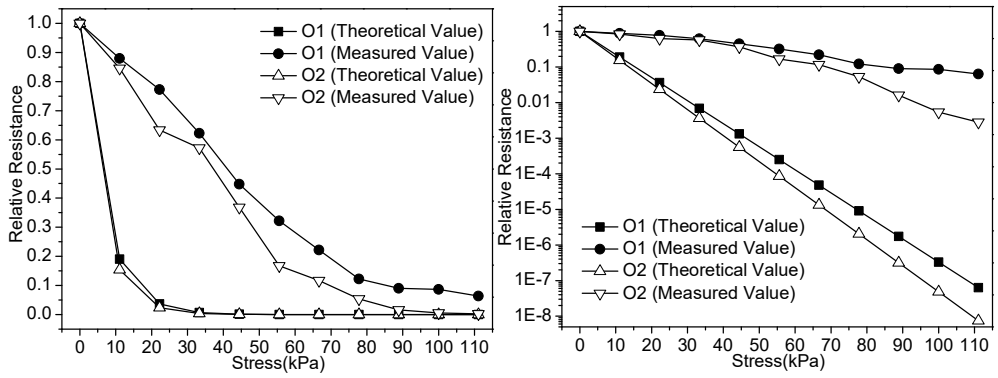

Fig.8 Comparison of the theoretical and measured piezoresistive properties of the MWCNT/silicone conductive foams

To verify the practicality of the piezoresistive model developed in this work, the theoretical variations of relative resistance of the O1 and O2 samples were calculated by the equations (6) accompanied with (3) and (5). The results were illustrated in the Fig.8 to compare to the measured relative resistance variations. The relative resistance-stress curves with a normal linear form were shown in the left part while those with a common logarithmic form were shown in the right part. Although the overall trends of the resistance changes matched, notable separations could be found between the theoretical values and the measured values no matter for the O1 or the O2 samples. The theoretically calculated relative resistances of both samples drop significantly under even a low stress and almost keep decreasing exponentially about 10^7 to 10^8 times under a stress of about 110kPa; on the contrary, the measured relative resistances dropped of less than 1000 times at the same stress. The resistance change was much less sensitive than the theoretical calculation, the main reason of which was thought as the viscoelasticity of the silicone matrix, which could severely weaken the interior deformation of the matrix and delay the approaching speeds of the adjacent MWCNT particles. The factor of the viscoelasticity will be considered to improve the accuracy of the piezoresistive model in our future works.

5. Conclusion

A series of novel MWCNT/silicone conductive foamed nanocomposites were fabricated with an OBSH, an ADCA and a $NaHCO_3$ type foaming agents. The porous structures of the foams, the distribution and orientation state of the MWCNTs in the silicone matrix were both observed with a laser microscope and SEM with or without a compressive load. It was found that the majority of the voids in the matrix crashed by the external pressure, which leaded to a reducing modulus and improved the piezoresistance of the composites. The contact and overlapping of the MWCNT particles were found dramatically enhanced by the pressure-caused reorientation, which was considered to be a main enhancement factor of the piezoresistive phenomenon of the MWCNT/silicone conductive foams. The most dense and fine porous structure was obtained by using the OBSH foaming agent which has the best affinity with the silicone elastomer and a highest foaming efficiency. The most sensitive piezoresistive property was obtained by the OBSH foamed MWCNT/silicone conductive nanocomposite. The overall trends of the resistance changes matched between the theoretical values and the measured values, however notable separations were found in their resistance-stress curves, which are thought to be caused by the viscoelasticity of the silicone matrix. The factor of the viscoelasticity will be

considered to improve the accuracy of the piezoresistive model in our future works, meanwhile more efficient foaming methods will be studied to further improve the piezoresistive property.

6. Acknowledgement

The authors gratefully acknowledge the support from Kitagawa Industries Co., Ltd. The authors also acknowledge the support from Advanced Low Carbon Technology Research and Development Program (ALCA) of Japan Science and Technology Agency (JST)-Japan.

References

1. R. George, K.T. Kashyap, R. Rahul, S. Yamdagni. Scr. Mater. 53, 1159-1163 (2005)

2. J.A. Kim, G.S. Dong, T.J. Kang, J.R. Youn. Carbon. 44, 1898-1905 (2006)

3. W.A. Curtin, B.W. Sheldon. Mater. Today. 7, 44-49 (2004)

4. S. Peng, K. Cho, P. Qi, H. Dai. Chem. Phys. Lett. 387, 271-276 (2004)

5. T.A. Saleh, V.K. Gupta. ESPR. 19, 1224-1228 (2012)

6. Y.S. Su, A. Manthiram. J. Chem. Soc., Chem. Commun. 48, 8817-8819 (2012)

7. E.F. Antunes, A.O. Lobo, E.J. Corat, V.J. Trava-Airoldi, A.A. Martin, C. Veríssimo. Carbon. 44, 2202-2211 (2006)

8. A.K. Kota, B.H. Cipriano, M.K. Duesterberg, A.L. Gershon, D. Powell, S.R. Raghavan, H.A. Bruck. Macromolecules. 40, 7400-7406 (2007)

9. S. Hong, S. Myung. Nat. Nanotechnol. 2, 207–208 (2007)

10. J.O. Aguilar, J.R. Bautista-Quijano, F. Avilés. Express Polym. Lett. 4, 292-299 (2010)

11. M.L. Yola, T. Eren, N. Atar. Biosens. Bioelectron. 60, 277-285 (2014)

12. F. Khaleghi, Z. Arab, V.K. Gupta, M. R. Ganjali, P.N. Atar, M.L. Yola. J. Mol. Liq. 221, 666-672 (2016)

13. J.A. Fishel, V.J. Santos, G.E. Loeb. In 2008 2nd IEEE RAS & EMBS International Conference on Biomedical Robotics and Biomechatronics. IEEE, 659-663 (2008)

14. C. Wei, L. Dai, A. Roy, T.B. Tolle. J. Am. Chem. Soc. 128, 1412-1413 (2006)

15. M.L. Yola, N. Atar. Electrochim. Acta. 119, 24-31 (2014)

16. K.M. Hassan, T.J. Fahimeh, N. Atar, M.L. Yola, V.K. Gupta, A.A. Ensafi. Ind. Eng. Chem. Res. 54, 3634-3639 (2015)

17. B. Ertan, T. Eren, İ. Ermiş, H. Saral, N. Atar, M.L. Yola. J. Colloid Interface Sci. 470, 14-21 (2016)

18. M. Park, H. Kim, J.P. Youngblood. Nanotechnology. 19, 055705 (2008)

19. M.H. Al-Saleh, U. Sundararaj. Carbon. 47, 1738-1746 (2009)

20. W.J. Kim, M. Taya, M.N. Nguyen. Mech. Mater. 41, 1116-1124 (2009)

21. G.D. Seidel, D.C. Lagoudas. J. Compos. Mater. 43, 917-941 (2009)

22. F. Carmona, R. Canet, P. Delhaes. J. Appl. Phys. 61, 2550-2557 (1987)

23. M. Taya, W.J. Kim, K. Ono. Mech. Mater. 28, 53-59 (1998)

24. F. Deng, Q. Zheng. Appl. Phys. Lett. 92, 071902 (2008)

25. X. Zhang, Y. Pan, Q. Zheng, X. Yi. J Polym Sci B Polym Phys. 38, 2739-2749 (2000)

26. X.W. Zhang, Y. Pan, Q. Zheng, X.S. Yi. Polym. Int. 50, 229-236 (2001)

27. C. Guo, Y. Kondo, C. Takai, M. Fuji. Polym. Int. (2016)